Wind-Blown Foliage and Human-Induced Fading in Ground-Surface Narrowband Communications at 400 MHz

Poh Kit Chong, *Member, IEEE*, Seong-Eun Yoo, Seong Hoon Kim, and Daeyoung Kim, *Member, IEEE*

***Abstract*—As small-scale fading is a spatial phenomenon, the movement of objects in the environment around static sensor nodes can induce significant fades. However, there have not been many works characterizing small-scale fading due to environmental factors for ground-surface wireless communications. We first measure the temporal fading characteristics experienced by antennas located just 1.5 cm above the surface of the ground due to wind-blown foliage or human movement in the environment for a narrowband channel in the 400-MHz frequency band. We then compare the extracted data to existing distributions and show that fading due to wind-blown foliage can be modeled as a Nakagami-m distribution, with wind speed and excess path-loss-dependent m shape factors. The α-μ distribution best characterizes the small-scale fading of a single human pedestrian, which is shown to have a repeatable pattern and can be up to 40 dB below the no-fading mean, whereas the Rician distribution, with an excess path-loss-dependent K-factor, can be used to characterize fading from multiple human pedestrians. We also report the second-order statistics of the average fade duration and the level crossing rate for fading caused by wind-blown foliage and multiple human pedestrians. Finally, we discuss the significance of the results on wireless sensor network protocol design and applications.**

***Index Terms*—Fading, ultra-high frequency (UHF) propagation, wireless sensor networks.**

I. Introduction

THE PHENOMENON of fading caused by the movement of foliage obstructing the line-of-sight (LOS) path between transmitter–receiver (T–R) pairs with elevated antennas has been studied in recent years for various frequency bands and different systems [1]–[7]. However, many sensor network applications [8] require nodes to be placed on the ground or other surfaces, which causes half of the first Fresnel zone to be obstructed. Furthermore, the Norton surface wave component of the ground wave cannot be ignored when the antenna is below one wavelength (λ) in height [9]. Hence, we are motivated to explore the temporal fading effects caused by wind-blown foliage and human movement experienced by ground-surface narrowband communications.

Previous attempts by Foran *et al.* [10] and Welch *et al.* [11] to characterize surface-level fading focused on the changes in heights of the antennas caused by specific human forms (standing, sitting on the floor, or lying prone), rather than for movement between static nodes. Joshi *et al.* [12] measured fading in foliated environments but with antenna heights of at least 75 cm above the surface of the ground. Sohrabi *et al.* [13] and Martínez-Sala *et al.* [14] both focused on estimating the path loss exponent for ground-surface communications rather than fading. We are not aware of any other work done so far to characterize fading experienced by ground-surface-level wireless communications caused by movement in the surrounding environment.

The objective of this paper is to perform experimental measurements of small-scale fading experienced by wireless devices located just above the surface of the ground, which is caused by movement in the surrounding environment for narrowband communications in the 400-MHz band, and to statistically characterize and model the fading channel. We first measure the fluctuation in signal strength at 70 locations in two different foliated environments over a period of 6 mo between mid-August 2009 to mid-February 2010, covering the seasons of fall and winter. The effects of wind speed ws and excess path loss Δ on the severity of fading caused by wind-blown foliage movement are observed, and we derive an empirical expression to represent the severity of the fading due to these factors. We then demonstrate that movement from a single human pedestrian is best characterized using the $\alpha-\mu$ distribution and that the fading from movements of multiple human pedestrians is Rician distributed based on 30 measurements performed over 15 days. The severity of fading caused by human movement can also be linked to static excess path loss. Finally, we discuss the implications on wireless sensor network protocol design.

The sections of this paper are organized as follows: Section II briefly describes our measurement setup and environment. Section III highlights the temporal fading characteristics of the

Manuscript received June 7, 2010; revised November 27, 2010 and February 12, 2011; accepted February 13, 2011. Date of publication March 10, 2011; date of current version May 16, 2011. This work was supported in part by a National Research Foundation of Korea Grant funded by the Korean government under Grant 2010-0018859 and in part by the Ministry of Knowledge Economy, Korea, under the Information Technology Research Center support program supervised by the National IT Industry Promotion Agency (NIPA) under Grant NIPA-2010-C1090-1021-0009. The review of this paper was coordinated by Prof. M. D. Yacoub.

P. K. Chong was with the Korea Advanced Institute of Science and Technology, Daejeon 305-701, Korea. He is now with Motorola Solutions, Penang 11950, Malaysia (e-mail: chongpohkit@ieee.org).

S.-E. Yoo was with the Korea Advanced Institute of Science and Technology, Daejeon 305-701, Korea. He is now with Daegu University, Gyeongsan 712-714, Korea (e-mail: seyoo@daegu.ac.kr).

S. H. Kim and D. Kim are with the Korea Advanced Institute of Science and Technology, Daejeon 305-701, Korea (e-mail: shkim08@kaist.ac.kr; kimd@kaist.ac.kr).

Color versions of one or more of the figures in this paper are available online at http://ieeexplore.ieee.org.

Digital Object Identifier 10.1109/TVT.2011.2125996

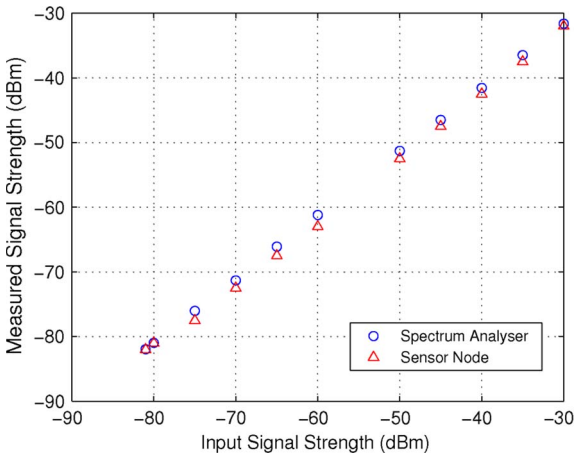

Fig. 1. Scatter plot of measured signal versus input signal.

signal caused by wind-blown foliage and presents an empirical representation of m as a function of average wind speed and excess path loss in fall and winter. The effects of human movement are shown in Section IV. Section V introduces some of the implications on existing sensor network protocols and simulation. Finally, we conclude in Section VI.

II. Measurement Equipment, Environment, and Methodology

A sinusoidal carrier wave (CW) transmitted at 10 dBm in the 400-MHz band was used as the signal source. As the receivers, we used a spectrum analyzer and sensor nodes to measure the amplitude of the CW. All the systems were equipped with the same type of $\lambda/4$ whip antenna with a 1.88-dBi gain. No ground planes were used to emulate realistic sensor node setups.

The spectrum analyzer was set to zero span with a 1-ms sweep time, and its video out signal was connected to a multimeter that was remotely controlled through the general purpose interface bus interface. The voltages corresponding to the peak marker traces were directly captured into a laptop at 200 samples/s. These voltages were then converted to the corresponding received power value. The (resolution) bandwidth and the video bandwidth of the spectrum analyzer were set to 10 and 30 kHz, respectively. The receiver sensor nodes were configured to measure the received signal strength indicator (RSSI) value every 5 ms as a single measurement or every 300 μs for 25 consecutive times every 50 ms as a burst measurement. The first setting allows a constant sampling of the channel and is similar to the sampling rate used in a previous work that characterized fading for wind-blown foliage [1], [4], whereas the second setting is used to determine the maximum amount of intrapacket fading in the channel within the time taken to transmit a single packet (a 64-B packet with an additional 8-B overhead takes approximately 7.5 ms to transmit at 76.8 kb/s).

The sensor nodes were calibrated using the spectrum analyzer, which has an amplitude accuracy of ± 2.03 dB at 0–55 °C for the 400-MHz frequency band. Fig. 1 shows the measured signal strength at the spectrum analyzer and sensor nodes versus the input signal strength after calibration. The sensor nodes give a relatively accurate value of the signal strength compared with the spectrum analyzer.

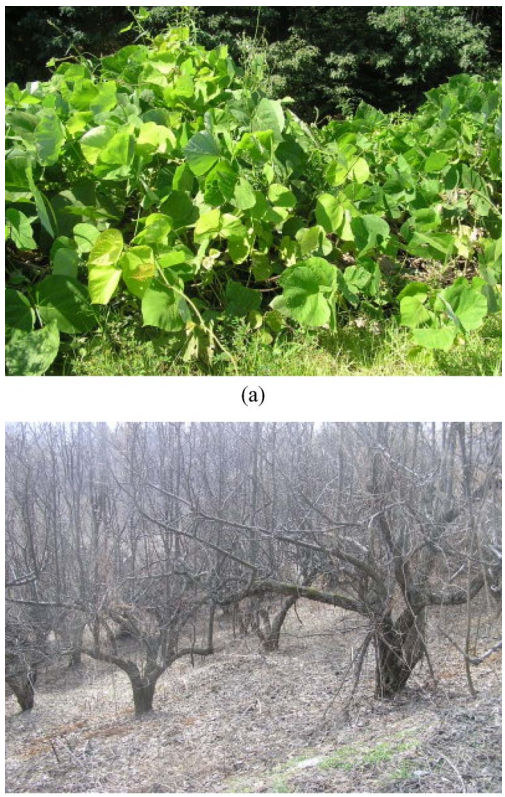

(a)

(b)

Fig. 2. Environment $\mathbb{H}$. (a) Mid-fall. (b) Late winter.

The average and maximum wind speeds were recorded every 15 s using a mobile weather station for measurements relating to wind-blown foliage movement. The anemometer is portable and was setup as close as possible to each measurement location since the wind is usually gusty and nonuniform within a large area. The accuracy of the anemometer is ± 0.18 m/s with a maximum speed of 56 m/s.

We performed the measurements in four different environments, detailed as follows:

1) Environment $\mathbb{H}$—A hilly area with slope gradients between 6° and 25°. The ground of the terrain is densely covered with creeping vegetation about 50–70 cm high. The leaves of the vegetation are broad and spade shaped with a length of 30 cm and a maximum width of 30 cm and are deciduous. The hills are also populated by a mix of trees with coniferous leaves, simple deciduous leaves, and simple nondeciduous leaves. The foliage in fall and winter is shown in Fig. 2.
2) Environment $\mathbb{P}$—A grassy plain that is covered in meter-high reedy grass and some small shrubs interspersed with some 3-m-tall petiolated compound leaf trees. The size of the leaves on the trees and shrubs is small with a surface area of around 15–50 cm^2, whereas the blades of the grass were around 30–40 cm long with a maximum width of 1 cm. The leaves on the trees and the shrubs are deciduous, whereas the grass dries up in winter. The foliage during fall is shown in Fig. 3.

Fig. 3. Environment $\mathbb{P}$ in mid-fall.

Fig. 4. Environment $\mathbb{F}$ in mid-fall.

Fig. 5. Environment $\mathbb{C}$ in mid-fall.

3) Environment $\mathbb{F}$—Two football fields next to each other measuring 50 m $\times$ 90 m and 60 m $\times$ 100 m, respectively. The fields are flat and sparsely covered with short grass (see Fig. 4).
4) Environment $\mathbb{C}$—Center of the campus near the plaza and the cafeteria with many human pedestrians with varying movements and speed. The ground was a mixture of bitumen road, cement tiles, and grass (see Fig. 5).

Measurements for foliated environments were performed in fall, when the foliage was densest, and in winter, after all the deciduous foliage had fallen for Environments $\mathbb{H}$ and $\mathbb{P}$

To measure the temporal fading from foliage and human movement, the base of the transmitter's antenna is first placed 1.5 cm above the ground at a selected location. The receiving antennas are then placed at a separate location, also at 1.5 cm above the ground surface, based on either a selected distance from the transmitter or a desired excess path loss over the average path loss measured from previous measurements [15]. Experimenters are always located at least 15 m away from the antennas during measurements to prevent any interference from human presence. Measurements of the effects of a single human movement were only performed on calm windless days, and only the person selected to cause fading approached the receivers or transmitter to try to exclude other possible sources of fading. Measurements for multiple humans were performed over a period of 15 days.

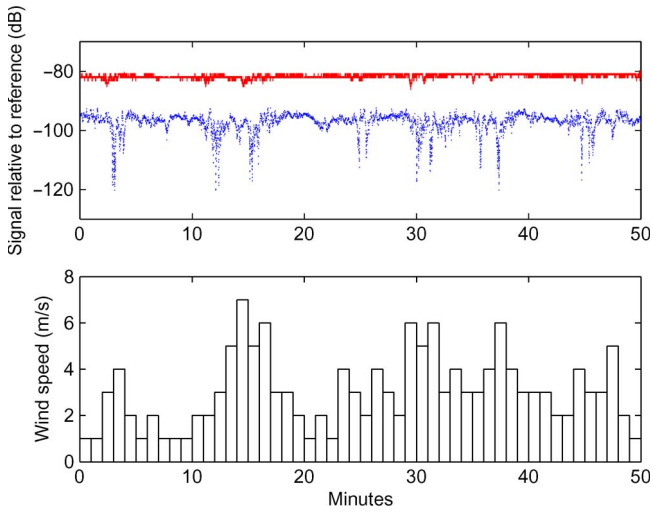

Fig. 6. Time-varying signal power (top) and average wind speed (bottom) on September 1, 2009.

III. Wind-Blown Foliage

Movement of wind-blown foliage can cause fading, as can be seen in Fig. 6, which shows the received signal power taken over a period of 50 min in windy conditions on September 1, 2009 at a location in Environment $\mathbb{H}$. However, the severity of the fades depends on the excess path loss as well as the wind speed. The red line (upper) in Fig. 6 is the fading recorded at a location with $\Delta_{\mathrm{dB}} = 0$ dB, whereas the blue line (lower) is the fading recorded at a nearby location with $\Delta_{\mathrm{dB}} = 18$ dB.

Fading in foliated channels (tree branches and leaves) has been characterized to be either Rician [2], [4], Nakagami-m [2], log-normal [3], or extreme value [3] distributed. These works measure the effects of fading using a reference signal located on a very high tower to a receiver at around human height above ground level for carrier frequencies of above 1 GHz. Meng *et al.* [16] found that fading in dense tropical foliage is either Rician or Gaussian distributed for very high frequency and subgigahertz ultra-high frequency (UHF) CWs using antennas located 2 m above the ground.

To characterize the fading caused by wind-blown foliage, we follow [2] and [4] by normalizing the measured signal envelope (amplitude) to its mean and statistically modeling the resulting values using the distribution functions previously mentioned and the flexible two-parameter $\alpha-\mu$ distribution [17]. To determine how well the measured and theoretical distributions fit, the root mean square error (RMSE) between the cumulative

TABLE I
AVERAGE RMSE FOR WIND-BLOWN FOLIAGE FADING DISTRIBUTIONS

Distribution / Environment	Rice	Rayleigh	Gaussian	Extreme Value	Log Normal	Nakagami-m	α-μ
$\mathbb{H}$	0.0495	0.0892	0.0496	0.0784	0.0507	0.0475	0.0471
$\mathbb{P}$	0.0488	0.1032	0.0487	0.0898	0.0515	0.0478	0.0473

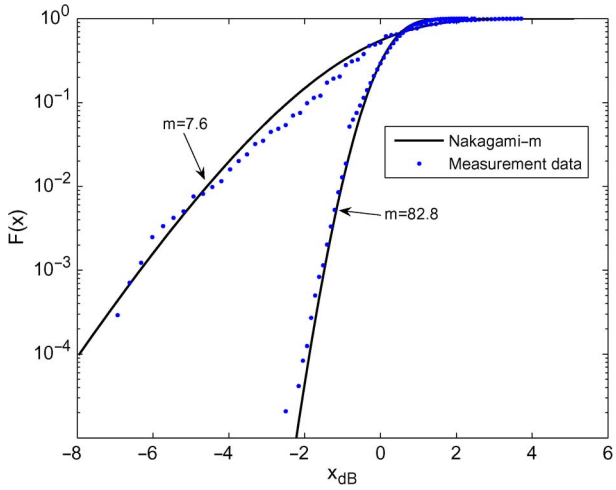

Fig. 7. CDF of measurement data compared with theoretical cdf for 4 min of samples from antenna locations with high and low excess path losses in Fig. 6. The curve for the high excess path loss (lower (blue) in Fig. 6) line has an $m = 7.6$, whereas the low excess path loss (upper (red) in Fig. 6) curve has an $m = 82.8$.

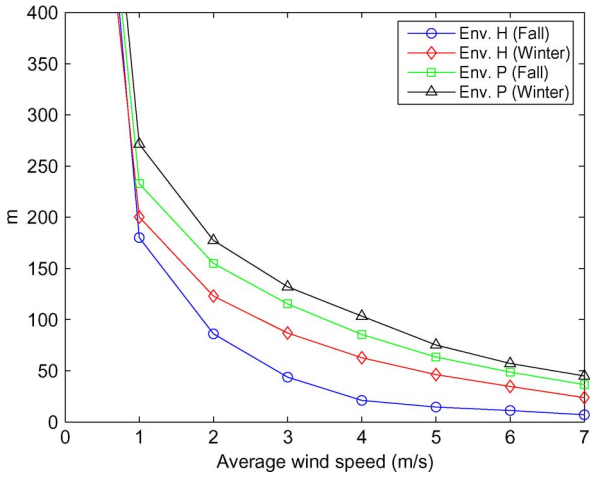

Fig. 8. Median m versus average wind speed.

distribution function (cdf) of the measurement data and the cdf of all the theoretical distributions is calculated as follows [4]:

$$\text{RMSE} = \sqrt{\frac{\sum_{i=1}^{N} E_i^2}{N}} \tag{1}$$

where N is the number of sample points, and E_i is the difference between the measured and theoretical cdfs at the same fading values. The average RMSE for all distributions is recorded in Table I. The distribution with the lowest RMSE is considered to be the distribution providing the best fit.

It can be observed from our measurements that the Nakagami-m [18] and $\alpha-\mu$ distributions give the best fit with the lowest RMSE values, with the $\alpha-\mu$ distribution giving a slightly better fit, and both distributions outperforming the Rice [19] and Gaussian distributions. However, we choose the Nakagami-m distribution to model the fading effects from the wind-blown foliage because the results from the Nakagami-m distribution fit both the first- and second-order statistics of the measurement results very well with one parameter less than the $\alpha-\mu$ distribution, although the $\alpha-\mu$ distribution provides a superior fit for the first-order statistics. Furthermore, the m shape factor of the Nakagami-m distribution can appropriately be characterized as a function of wind-speed and excess path loss, which we will show later in this section. It should be noted that the results shown in Table I are for windy conditions. During calm conditions with no wind, there is hardly any variation in signal strength recorded, and it can be assume that no fading occurs (i.e., a delta function). Fig. 7 show the cdf plot of the first 4 min from Fig. 6 compared with the theoretical cdfs of the Nakagami-m distribution. The Nakagami-m probability density function (pdf) of the signal envelope r is [20]

$$p_N(r) = \frac{2m^m r^{2m-1}}{\Gamma(m)\Omega^m} e^{\frac{-mr^2}{\Omega}} \tag{2}$$

where m is the Nakagami shape factor, Ω is the average signal power, and Γ is the Gamma function. m is related to the Rice distribution's K-factor by $m \approx (1+K)^2/2K+1$ for $m \geq 1$, and a Nakagami-m distribution can be *approximated* by a Rician distribution as [20]

$$p_R(r) = \frac{2(K+1)r}{\Omega} e^{\left(-K-\frac{(K+1)r^2}{\Omega}\right)} I_0\left(2\sqrt{\frac{K(K+1)}{\Omega}}r\right) \quad r, K, \Omega \geq 0 \tag{3}$$

where $I_0(\cdot)$ is the zeroth-order modified Bessel function of the first kind, and K and Ω are the shape and scale parameters, respectively. K is the ratio of the power received via the dominant path to the power contribution of the random paths, and $\Omega = E[r^2]$ is the average signal power, where $r(t)$ is the received signal envelope.

We first estimate m using the inverse normalized variance estimator [20] from 4-min measurement samples of 48 000 points each. Then, these were binned according to the average wind speed $\overline{ws} = [0, 1, 2, \ldots, 7] \pm 0.5$ m/s measured over the same period. By plotting the median m for each bin, we can derive a statistical model for the distribution of the m shape factor. Fig. 8 shows the median m for our measured data in each $\overline{ws}$ bin in the $\mathbb{H}$ and $\mathbb{P}$ environments in fall and winter. The median m can be seen to exponentially decay according to $\overline{ws}$ for all environments and season. The effect of the wind is more significant when changing from no wind to moderate wind

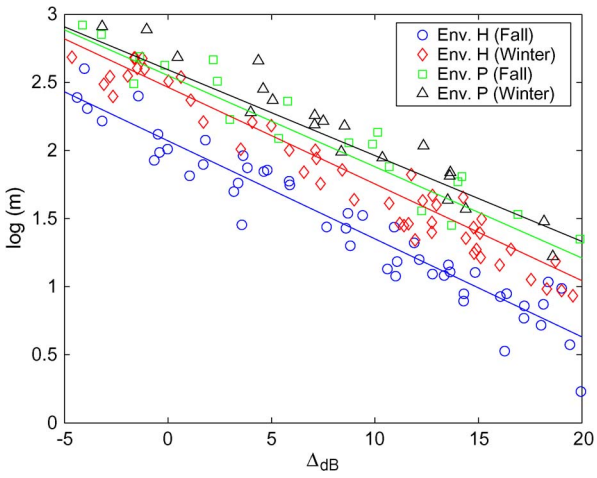

Fig. 9. $\log(m)$ versus Δ_{dB} at $\overline{ws} = 3$ for Environments $\mathbb{H}$ and $\mathbb{P}$ in fall and winter.

speed than when going from moderate to high wind speeds. A large variance was also observed around each median data due to factors such as wind direction or Δ at each location. This is because a change in wind direction may affect the severity of fading, even if the wind magnitude remains unchanged, due to the changing of the foliage angles. However, the median m shows a strong correlation to $\overline{ws}$.

Fig. 6 highlighted the effects of excess path loss on the severity of fading caused by wind-blown foliage. We found that distance is not an important factor in determining the severity of the fades for our results. To determine the effects of excess path loss, we first determined the excess path loss Δ_{dB} (in decibels) at each sample location by comparing the measured signal strength with regard to the average for that distance and terrain profile using data from prior measurements [15]. We then compared the estimated m values to Δ_{dB} for each sample. Fig. 9 shows the median m for $\overline{ws} = 3$ m/s at Environments $\mathbb{H}$ and $\mathbb{P}$ in fall and winter plotted against the Δ_{dB} for each sample location. By plotting the values of m in logarithmic, a strong negative linear correlation between $\log(m)$ and Δ_{dB} (the log symbol is used to represent a base-10 logarithm) can be seen. Measurements for other $\overline{ws}$ show a similar linear relationship between $\log(m)$ and Δ_{dB}. Since no fading occurs when $\overline{ws} = 0$ m/s, we omit the results from our analysis. As the median m decays exponentially according to $\overline{ws}$ (Fig. 6), we use MATLAB to perform multiple regression for $\log(m)$ as a function of $\overline{ws}$ and Δ_{dB}. The median m can then be represented as a function of $\overline{ws}$ and Δ_{dB} as follows:

$$\log(m) = C_2\overline{ws} + C_1\Delta_{\mathrm{dB}} + C_0$$

or

$$m = \Delta^{10C_1} 10^{(C_2\overline{ws}+C_0)} \tag{4}$$

where C_2, C_1, and C_0 are the regression coefficients depending on the season and environment, with a minimum value of m of 0.5. The values of the coefficients for both environments are summarized in Table II. The coefficients show that Environment $\mathbb{P}$ is less affected by foliage movement compared with Environment $\mathbb{H}$ and has coefficients relatively similar to

TABLE II
C_0,C_1, AND C_2 VALUES

	C_0	C_1	C_2
Location $\mathbb{H}$ (fall)	2.752	-0.072	-0.227
Location $\mathbb{H}$ (winter)	2.902	-0.071	-0.146
Location $\mathbb{P}$ (fall)	2.944	-0.067	-0.131
Location $\mathbb{P}$ (winter)	2.968	-0.063	-0.125

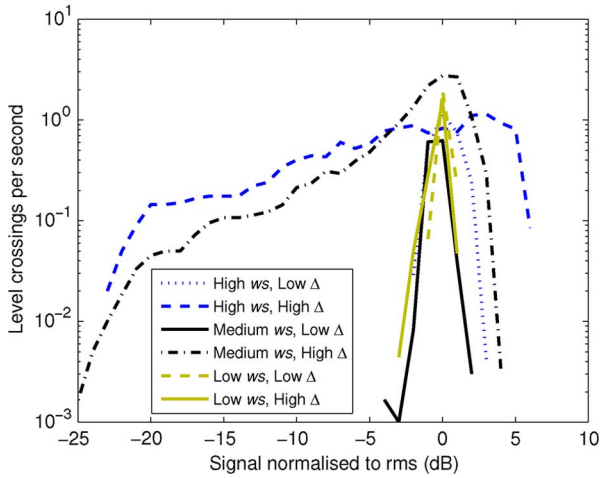

Fig. 10. LCRs. The estimated m values for the plots are 35.14, 0.95, 63.45, 3.3, 106.52, and 49.37 for the scenarios listed top-down in the legend.

Environment $\mathbb{H}$ during winter when only some of the trees still have leaves. We speculate that this is due to the foliage in Environment $\mathbb{H}$ having a larger surface and being more dense, thus scattering the diffracted and reflected signals more effectively.

The level crossing rates (LCRs) are defined as the rate of which a fading signal envelope crosses a level in a positive going direction. The LCRs derived from two receivers positioned within $\lambda/2$ of each other but with different Δ_{dB} for high (6–7 m/s), medium (3–5 m/s), and low (1–2 m/s) ws are shown in Fig. 10. High and low Δ's are 12.2 and 1.7 dB above the predicted average, respectively. The signal variation is higher and occurs more often when ws increases and is more significant with higher Δ_{dB}, as can be seen from the larger spreads. Fig. 11 shows the comparison between the measured LCR and the theoretical closed-form Nakagami-m LCR formula obtained from [21]. We omit the results of the low Δ, because they are quite similar to the low ws, as well as to reduce clutter.

The average fade duration (AFD) is defined as the average period of time a received signal is below a specified level. The AFD shows that when Δ is high, faster winds can cause significant changes to the received signal for longer durations, whereas in other conditions, the received RF signal fades for less time (see Fig. 12). The shapes of the curves for high and medium winds with high Δ are quite similar, showing that wind speed has less effect on the AFD after a certain level. The "Z" shape seen in the curves for low $\overline{ws}$ and/or low Δ indicates that the RF signal tends to fluctuate constantly about a small range in these conditions. Fig. 13 shows the comparison between the measured AFD versus the theoretical Nakagami-m

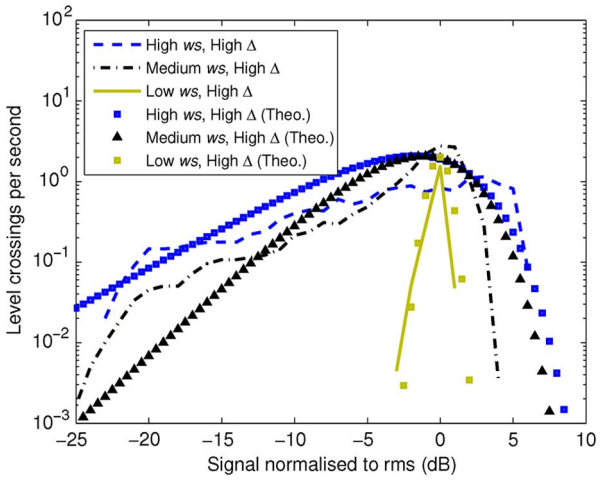

Fig. 11. Measured versus simulated LCRs. The estimated m values for the plots are 0.95, 3.3, and 49.37 for the high, medium, and low wind speeds, respectively.

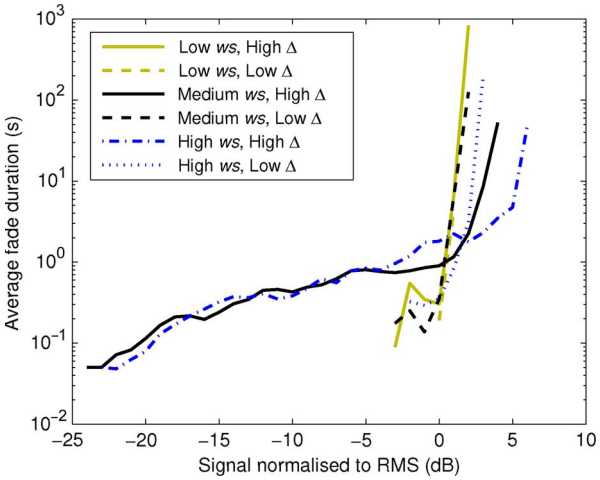

Fig. 12. AFD.

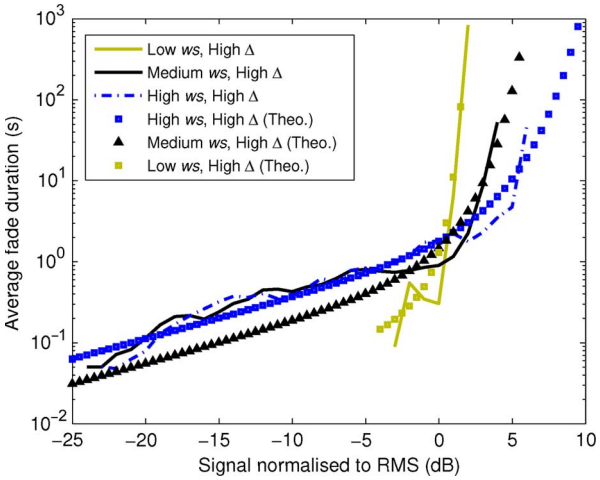

Fig. 13. Measured versus simulated AFD.

AFD obtained from [21]. Similar to the LCR graphs, we omit the results of the low Δ.

The top graph in Fig. 14 shows the signal variation recorded within a burst measurement, whereas the bottom graph shows

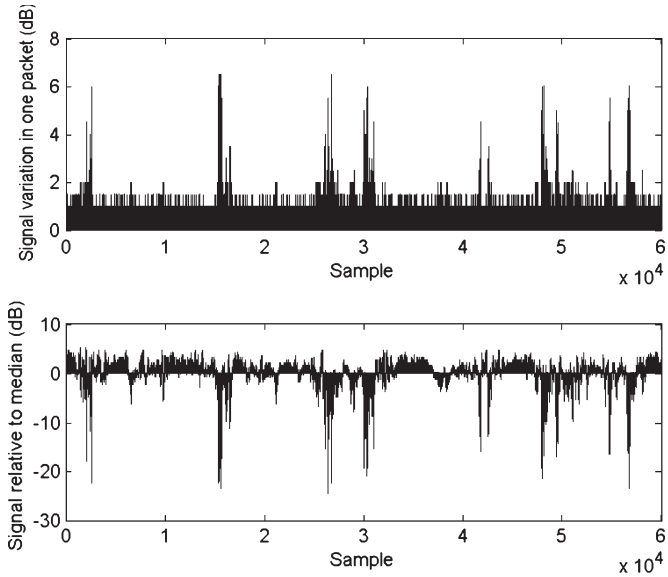

Fig. 14. Signal variation within a burst measurement (top) and average signal strength in a burst measurement relative to the median for all measurements.

the average signal strength of the envelope for each burst relative to the median signal strength for all burst measurements. These graphs show that the channel is usually coherent and has little variation in signal strength throughout the time taken to receive a single packet in wireless sensor networks, except when deep fades occur, and confirms the LCR and AFD results. During deep fades, the received power recorded over a single burst measurement may vary by up to 6 dB.

IV. Human Movement

Similar to wind-blown foliage, human movement in the vicinity of a T–R pair can also cause fading. However, the fading effects caused by human movement are more difficult to classify compared with wind-blown foliage as there is a very wide range of possible movements, velocity, and positions that a person can make as well as the effects of different numbers of people. We perform measurements at Environment $\mathbb{F}$ for a human walking perpendicular ($\perp$) or parallel ($\parallel$) to the LOS path. In these experiments, the T–R pairs were separated by a distance of 10, 20, or 30 m. We ensured that the received signal strength was near the predicted average value to remove the effects of excess path loss.

For the perpendicular movements, a person walked along a 10-m route perpendicular to the LOS path of the T–R pair at a consistent speed of 0.67 m/s, with the middle of the route intersecting the LOS path. The route for the first measurement was across the face of the transmitter, with each subsequent route spaced 2.5 m away from the transmitter and toward the receiver before the final route ended across the face of the receiver.

For the parallel movements, a person walked along a route parallel to the LOS path, starting at 5 m behind the transmitter and ending 5 m behind the receiver. The first route started on the LOS path, with the subsequent routes spaced at multiples of 1.5 m away from the LOS path.

TABLE III
AVERAGE RMSE FOR FADING DISTRIBUTIONS FOR SINGLE HUMAN MOVEMENT

Distribution	Rice	Rayleigh	Gaussian	Extreme Value	Log Normal	Nakagami-m	α-μ
RMSE (all)	0.0721	0.1154	0.0722	0.0763	0.0761	0.0728	0.0331
RMSE$_\perp$	0.0707	0.1166	0.0708	0.0772	0.0746	0.0713	0.0321
RMSE$_\parallel$	0.0755	0.1125	0.0758	0.0739	0.0797	0.0766	0.0338

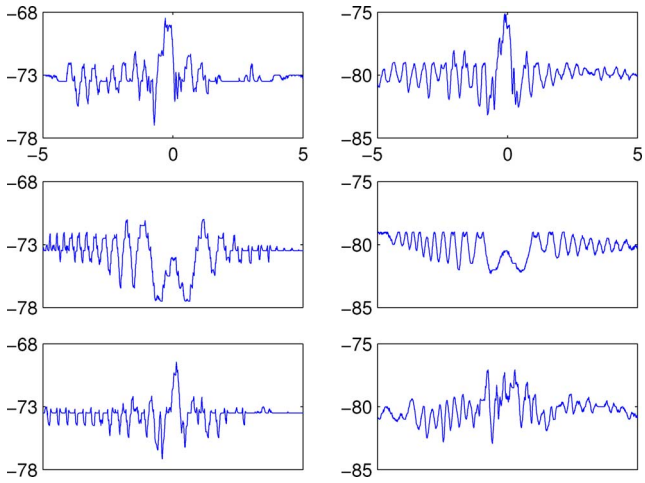

Fig. 15. Fading effects that occur when a human walks along a 10-m route perpendicular to a T–R pair's LOS path. 0 position on the x-axis is the intersection between the route and the LOS path. The T–R distances are 20 and 30 m for the left and right columns, respectively. The first, second, and third rows are when the intersection is just in front of T, right in between T–R, and just in front of R, respectively.

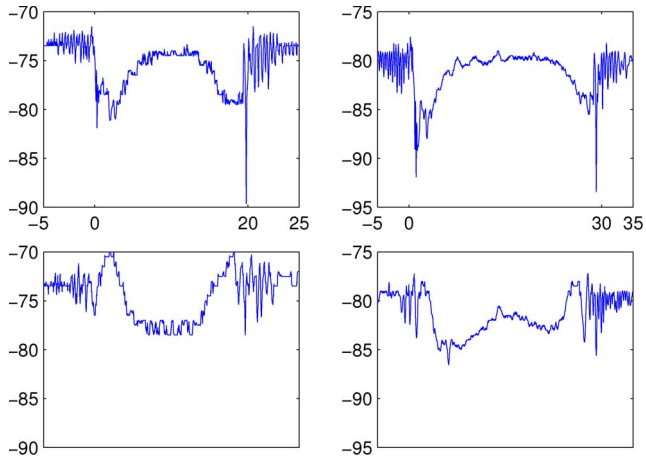

Fig. 16. Fading effects that occur when a human walks along a route parallel to a T–R pair's LOS path. 0 position on the x-axis is the position of T. The human route begins 5 m behind the transmitter and ends 5 m behind the receiver. The T–R distances are 20 and 30 m for the left and right columns, respectively. The first row is when the human walks right on the LOS path (i.e., directly between the nodes), whereas the second is when the parallel route is 1.5 m to the side of the LOS path.

Table III shows the average RMSE between the theoretical and measured fading distributions for these experiments. The fading that occurs when a single pedestrian walks near a T–R pair can be fitted to any one of the Rician, Gaussian, Nakagami-m, lognormal, or extreme value distributions, depending on the route and the LOS path. Conversely, along another route, the same distribution would give a very poor fit. As such, the $\alpha-\mu$ distribution is used to characterize the fading because of its flexibility. This distribution includes the Nakagami-m, Rayleigh, exponential, Weibull, one-sided Gaussian, Gamma, Chi (the discrete version of Nakagami-m), Erlang, and central Chi-squared (the last two are both the discrete versions of the Gamma distribution). The $\alpha-\mu$ pdf of the signal envelope r is [17]

$$p_{\alpha-\mu}(r) = \frac{\alpha\mu^{\mu} r^{\alpha\mu-1}}{\hat{r}^{\alpha\mu}\Gamma(\mu)} e^{-\mu\left(\frac{r}{\hat{r}}\right)^{\alpha}} \tag{5}$$

where $\alpha > 0$ is an arbitrary parameter, $\hat{r} = \sqrt[\alpha]{E(r^{\alpha})}$, and $\mu = E^2(r^{\alpha})/V(r^{\alpha})$. The flexibility of the $\alpha-\mu$ distribution allows better fitting of measurement data for the single pedestrian compared with other distributions.

Fig. 15 shows the fading experienced for a T–R pair at 20 and 30 m for the perpendicular movement experiments. Fig. 16 shows the fading that occurs when a person walks along a route parallel to the T–R pair at Environment $\mathbb{P}$. The left and right columns of the figure are for T–R separations of 20 and 30 m, respectively. For both measurements, there seems to be a pattern to fading, regardless of the separation of the LOS path.

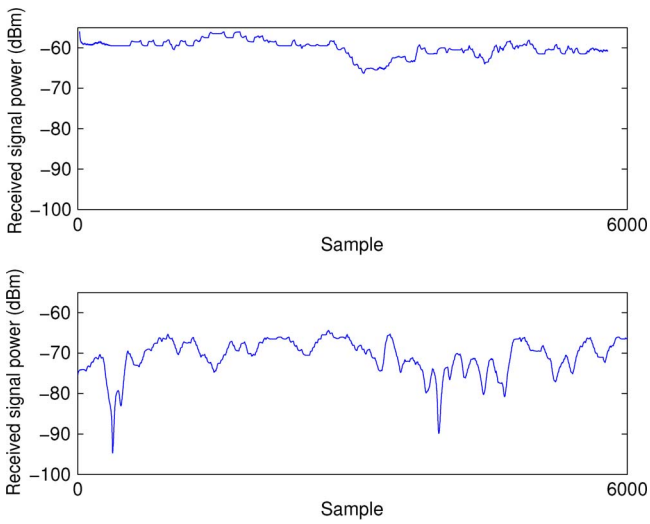

Fig. 17. Fading effects that occur due to random human movements such as walking, squatting, or twisting the upper torso. The upper figure has $\Delta_{\mathrm{dB}} = -0.7$ dB, whereas the lower figure's $\Delta_{\mathrm{dB}} = 9.1$ dB. Both positions are within $\lambda/2$ of each other.

The intensity of fades caused by human movement is also correlated with the excess path loss. Positions with higher Δ tend to suffer more intense fades. Fig. 17 shows the fading that occurs due to random human movement such as walking, squatting and standing, changing body posture, or twisting the upper torso behind a receiver. For this measurement, the same T–R pair was used to avoid hardware differences. The receiver is first

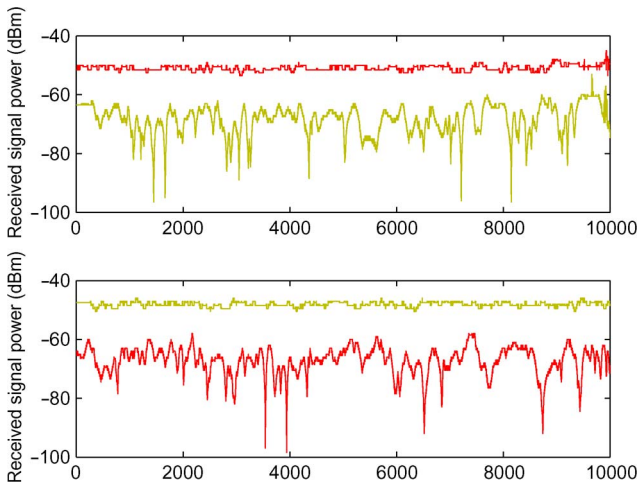

Fig. 18. Fading effects that occur due to random human movements indoors. The positions of two nodes are swapped for the top and bottom graphs. The first node is represented by the red line (upper in top subfigure and lower in bottom subfigure), and the second node is represented by the yellow line (lower in top subfigure and upper in bottom subfigure).

placed in a position on the ground in Location $\mathbb{H}$ with a path loss near the predicted average, and a person performed the movements described above behind the receiver. Next, another position with high Δ within $\lambda/2$ away was selected for the second measurement, and the same person repeated the movements.

A similar experiment was repeated indoors using a transmitter and two receiver nodes. The transmitter was placed inside the bottom shelf of a metal cabinet with the doors closed, causing all received signal outside to be multipath signals. The first receiver was placed in a position of low Δ outside the cabinet, whereas the second was placed within $\lambda/2$ away in a position with around 15 dB lower reception power relative to the first node. A person then randomly moved around the room. Next, we swapped the two nodes and again performed random human movement around the area. The top graph in Fig. 18 shows the result of the first measurement, whereas the bottom graph shows the result after the swap. The results suggest that the intensity of fading depends on the excess path loss of the position rather than on the hardware or distance. The effects of fading due to human movement are also not strongly correlated, even for nearby positions. The results also show why RSSI values cannot be used alone to determine link stability, and links with seemingly high RSSI values experience periodic packet losses.

For fading caused by multiple human pedestrians moving at various speeds and directions, we performed the measurements at Environment $\mathbb{C}$ at the center of our campus near the cafeteria and plaza using measurements from three antennas in a row with a separation of $\lambda/4$. The fading was found to be best fitted with a Rician distribution (see Table IV), with a K-factor (see Fig. 19) that is dependent on Δ_{dB}, i.e.,

$$K_{\mathrm{dB}} = -1.218\ \Delta_{\mathrm{dB}} + 14.5246. \tag{6}$$

Although the RMSE values for the Rice and Nakagami-m distributions are quite close, inspection of second-order statistics for both distributions shows that the Rician distribution gives the best fit in this scenario. For example, we plot the theoretical LCR and AFD for the Rice [22] and Nakagami-m [21] distributions for the high excess path loss data in Figs. 20 and 21 using the m and K values estimated from experimental data. As can be seen, the Rice model gives a better fit compared with the Nakagami-m model.

The LCR and AFD for multiple human pedestrians with different Δ_{dB} are also shown in Figs. 20 and 21, respectively. Links with higher Δ tend to suffer more frequent, longer, and more severe fades compared with links with low Δ. However, they also have longer and more frequent higher positive fades that increase the signal reception.

V. Implication of Results on Wireless Sensor Network Protocols and Deployment

Based on the measurement results presented here, we discuss the following implications to current wireless sensor network (WSN) deployment, protocol design, or parameter selection.

1) Energy is a limited and extremely important resource for WSNs. However, for nodes to determine stable links, periodic transmission and reception of probe packets that consume a lot of energy have to be performed to gather information for routing metrics such as expected transmission count (EXT) [23]. By prioritizing transmission on links with low excess path loss, the periodicity of such probes can be optimized to suit the local environment (i.e., choosing a periodicity where changes to the environment are expected to affect the excess path loss between links).
2) Error correction codes such as forward error correction can selectively be used between links that have high Δ to improve reliability and can be neglected for links with low Δ. Furthermore, techniques such as bit interleaving can help to improve data reception, particularly since the AFD of deep fades lasts only for a very short duration and affects a small cluster of consecutive bits.
3) Protocols that rely on short channel sampling to determine channel occupancy may need to tune their thresholds or sampling frequency in locations with foliage or human movement. For example, sampling the channel just once or twice in quick succession (on the order of μs) may lead to the mistaken assumption that the channel is clear, thus leading to packet collision or missing an incoming packet. The transmission of a string of preamble packets (e.g., B-MAC + [24]) could also be used by neighboring nodes as a means to determining the stability of the link in foliated or human-movement environments rather than being considered as a source of energy wastage through overhearing.
4) To maximize energy efficiency, WSN protocols tend to pick the next hop that is closest to the destination. A careful evaluation of how next-hop node selection thresholds are chosen needs to be done based on the environmental factors. For example, the presence of a single human may cause fades of up to 15 dB even for links with low Δ (see Fig. 16) and up to 40 dB for links with high Δ (see Fig. 18). Longer links may also have a higher probability of more human interference and suffer even

TABLE IV
AVERAGE RMSE FOR FADING DISTRIBUTIONS WITH MULTIPLE HUMANS

Distribution	Rice	Rayleigh	Gaussian	Extreme Value	Log Normal	Nakagami-m
RMSE	0.0201	0.0454	0.0206	0.0363	0.0368	0.0209

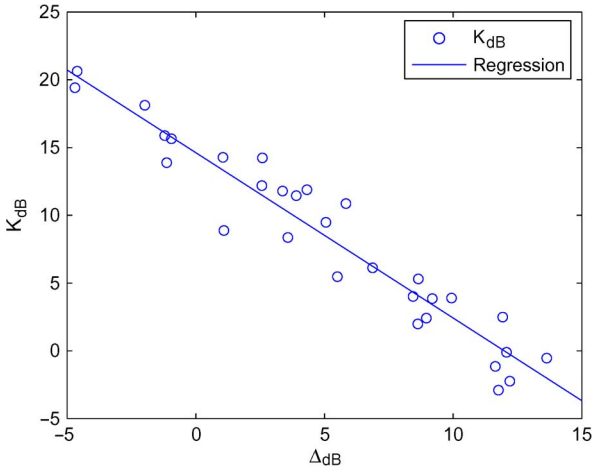

Fig. 19. Intensity of fading with multiple humans versus excess path loss in decibels.

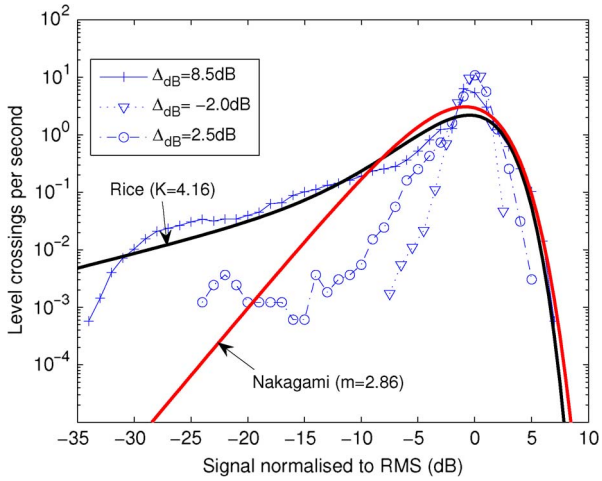

Fig. 20. LCRs for multiple humans. The theoretical LCRs for the Rice and Nakagami models are shown for the high excess path loss plot.

more significant or frequent fades. A distance-dependent fade margin may need to be considered in areas with these scenarios.

5) Opportunistic protocols that take try to advantage of node diversity or channel conditions may be better served by prioritizing forwarders with low Δ in environments with high foliage or human movement or to use short transmissions to take advantage of immediate channel conditions. In more calm environments, forwarders with higher Δ can be used as well since the links become more predictable.

VI. CONCLUSION AND FUTURE WORK

We have presented the measurement results of small-scale fading for surface-level narrowband communications in the

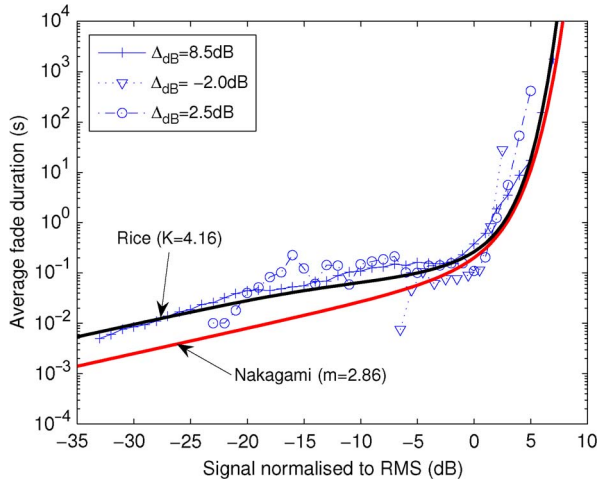

Fig. 21. AFD for multiple humans. The theoretical AFDs for the Rice and Nakagami models are shown for the high excess path loss plot.

400-MHz UHF band caused by wind-blown foliage and human movement outdoors in different terrains. We have shown that the fading caused by wind-blown foliage can be characterized as a Nakagami-m distribution with the m shape factor a function of both wind speed and excess path loss, and we derive an empirical expression of m as a function of these two factors. Aside from the average wind speed and the excess path loss, we also showed that m is affected by the foliage type and the different seasons, and we give the parameters to determine the average m for Environments $\mathbb{H}$ and $\mathbb{P}$ in fall and winter.

The effects of a single human movement can be fitted using the flexible $\alpha-\mu$ distribution, whereas the fading caused by movement from multiple human pedestrians can be characterized well as a Rician distribution with the severity of the fading dependent on the excess path loss of each T–R pair. Antennas in positions with high excess path loss suffer more severe fades, where even small changes in a human posture or position can lead to fades of up to 40 dB below the no-fading average. Therefore, it can be concluded that choosing low excess path loss links will generally lead to more stable communication.

While the results presented here are for measurements performed in the 400-MHz band, we believe that similar fading characteristics can be seen for the entire UHF band, including the ISM frequencies in the UHF band, particularly for pedestrian-induced fading, since the size of pedestrians is large compared with the wavelengths in the band. For foliage-induced fading, the size of foliage relative to λ might affect the characteristics of fading at other frequencies. We plan to verify this in future work by performing more detailed experiments in different bands. In addition to this, we also plan to explore the effects of rainfall on ground-surface narrowband communications in the 400-MHz band to determine if heavy and continuous rainfall affects the fading characteristics by

temporarily changing the permittivity and conductivity of the ground due to the absorption and/or pooling of water on the surface of the ground.

ACKNOWLEDGMENT

The authors would like to thank and acknowledge the three anonymous reviewers and the Associate Editor for their invaluable comments and suggestions, which substantially improved this paper.

REFERENCES

[1] A. Kajiwara, "LMDS radio channel obstructed by foliage," in *Proc. IEEE Int. Conf. Commun.*, 2000, vol. 3, pp. 1583–1587.
[2] J. C. R. Dal Bello, G. L. Siqueira, and H. L. Bertoni, "Theoretical analysis and measurement results of vegetation effects on path loss for mobile cellular communication systems," *IEEE Trans. Veh. Technol.*, vol. 49, no. 4, pp. 1285–1293, Jul. 2000.
[3] S. Perras and L. Bouchard, "Fading characteristics of RF signals due to foliage in frequency bands from 2 to 60 GHz," in *Proc. 5th Int. Symp. Wireless Pers. Multimedia Commun.*, Oct. 2002, vol. 1, pp. 267–271.
[4] M. H. Hashim and S. Stavrou, "Wind influence on radio waves propagating through vegetation at 1.8 GHz," *IEEE Antennas Wireless Propag. Lett.*, vol. 4, no. 1, pp. 143–146, 2005.
[5] D. Crosby, V. S. Abhayawardhana, I. J. Wassell, M. G. Brown, and M. P. Sellars, "Time variability of the foliated fixed wireless access channel at 3.5 GHz," in *Proc. 61st IEEE Veh. Technol. Conf.*, 2005, vol. 1, pp. 106–110.
[6] Y. Zhang and D. G. Michelson, "Impact of wind-induced fading on the capacity of point-to-multipoint fixed wireless access systems," in *Proc. Int. Conf. Wireless Commun. Mobile Comput.*, 2006, pp. 979–984.
[7] Y. S. Meng, Y. H. Lee, and B. C. Ng, "The effects of tropical weather on radio-wave propagation over foliage channel," *IEEE Trans. Veh. Technol.*, vol. 58, no. 8, pp. 4023–4030, Oct. 2009.
[8] S. Yoo, P. K. Chong, and D. Kim. (2009). S3: School zone safety system based on wireless sensor network. *Sensors*. [Online]. *9(8)*, pp. 5968–5988. Available: http://www.mdpi.com/1424-8220/9/8/5968/
[9] K. Bullington, "Radio propagation at frequencies above 30 megacycles," *Proc. IRE*, vol. 35, no. 10, pp. 1122–1136, Oct. 1947.
[10] R. A. Foran, T. B. Welch, and M. J. Walker, "Very near ground radio frequency propagation measurements and analysis for military applications," in *Proc. IEEE Mil. Commun. Conf.*, 1999, vol. 1, pp. 336–340.
[11] T. B. Welch, J. R. Wood, R. W. McParlin, L. K. Schulze, T. P. Flaherty, III, S. G. Carlone Hanson, R. J. Cahill, and R. A. Foran, "Very near ground RF propagation measurements for wireless systems," in *Proc. IEEE Mil. Commun. Conf.*, 2000, vol. 3, pp. 2556–2558.
[12] G. G. Joshi, C. B. Dietrich, C. R. Anderson, W. G. Newhall, W. A. Davis, J. Isaacs, and G. Barnett, "Near-ground channel measurements over line-of-sight and forested paths," *Proc. Inst. Elect. Eng.—Microw., Antennas Propag.*, vol. 152, no. 6, pp. 589–596, Dec. 2005.
[13] K. Sohrabi, B. Manriquez, and G. J. Pottie, "Near ground wideband channel measurement in 800–1000 MHz," in *Proc. 49th IEEE Veh. Technol. Conf.*, Jul. 1999, vol. 1, pp. 571–574.
[14] A. Martínez-Sala, J.-M. Molina-Garcia-Pardo, E. Egea-Lopez, J. Vales-Alonso, L. Juan-Llacer, and J. Garcia-Haro, "An accurate radio channel model for wireless sensor networks simulation," *J. Commun. Netw.*, vol. 7, no. 4, pp. 401–407, Dec. 2005.
[15] P. K. Chong and D. Kim, "Surface-level path loss modelling for sensor networks in flat and irregular terrain," Korea Advanced Inst. Sci. Technol., Daejeon, Korea, Tech. Rep. CS/TR-2010-327, 2010.
[16] Y. S. Meng, Y. H. Lee, B. C. Ng, and S. Y. Huang, "Wind and rain influences on forested radiowave propagation," in *Proc. IEEE Antennas Propag. Soc. Int. Symp.*, Jun. 2007, pp. 3748–3751.
[17] M. D. Yacoub, "The $\alpha-\mu$ distribution: A physical fading model for the stacy distribution," *IEEE Trans. Veh. Technol.*, vol. 56, no. 1, pp. 27–34, Jan. 2007.
[18] M. Nakagami, "The m-distribution—A general formula of intensity distribution of rapid fading," in *Statistical Methods in Radio Wave Propagation*, W. Hoffman, Ed. New York: Pergamon, 1960, pp. 3–36.
[19] S. O. Rice, "Statistical properties of a sine wave plus random noise," *Bell Syst. Tech. J.*, vol. 27, no. 1, pp. 109–157, Jan. 1948.
[20] A. Abdi and M. Kaveh, "Performance comparison of three different estimators for the Nakagami m parameter using Monte Carlo simulation," *IEEE Commun. Lett.*, vol. 4, no. 4, pp. 119–121, Apr. 2000.
[21] M. D. Yacoub, J. E. V. Bautista, and L. Guerra de Rezende Guedes, "On higher order statistics of the Nakagami-m distribution," *IEEE Trans. Veh. Technol.*, vol. 48, no. 3, pp. 790–794, May 1999.
[22] T. S. Rappaport, *Wireless Communications: Principles and Practice*. Upper Saddle River, NJ: Prentice-Hall, 2001.
[23] D. S. J. De Couto, D. Aguayo, J. Bicket, and R. Morris, "A high-throughput path metric for multi-hop wireless routing," in *Proc. 9th Annu. Int. Conf. Mobile Comput. Netw.*, 2003, pp. 134–146.
[24] M. Awenuti, P. Corsini, P. Masci, and A. Vecchio, "Increasing the efficiency of preamble sampling protocols for wireless sensor networks," in *Proc. 1st Mobile Comput. Wireless Commun. Int. Conf.*, Sep. 2006, pp. 117–122.

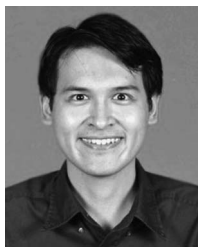

Poh Kit Chong (M'99) was born in Malaysia in 1979. He received the B.Eng. degree in electronics from Universiti Teknologi Malaysia, Johor Bahru, Malaysia, in 2001, the M.Eng.Sc. degree from Multimedia University (MMU), Cyberjaya, Malaysia, in 2003, and the Ph.D. degree in information and communications engineering from the Korea Advanced Institute of Science and Technology, Daejeon, Korea, in 2010.

He was a Research Scholar with MMU from 2001 to 2003 and a Network Software Engineer with Intel from 2003 to 2005 before embarking on his Ph.D. studies. He is currently a Senior Staff Engineer with Motorola Solutions, Penang, Malaysia. His current research interests include wireless channel measurement and modeling, communication protocols, and embedded systems.

Dr. Chong is a Reviewer for the IEEE COMMUNICATION LETTERS and the IEEE TRANSACTIONS ON VEHICULAR TECHNOLOGY.

Seong-Eun Yoo received the B.E. degree in electronics and computer engineering from Hanyang University, Seoul, Korea, in 2003, the M.S. degree in computer science and engineering from the Information and Communications University, Daejeon, Korea, in 2005, and the Ph.D. degree in information and communications engineering from the Korea Advanced Institute of Science and Technology, Daejeon, in 2010.

He was a Software Engineer with Fine Digital, Inc., from July 1999 to January 2002 and a Research Engineer with Sensor Networks Research, Inc. from March 2006 to February 2009. He was a Postdoctoral Researcher with the Information and Electronics Research Institute, KAIST, from February to August in 2010. Since September 2010, he has been a faculty member with the School of Computer and Communication Engineering, Daegu University, Gyeongsan, Korea. His research interests include real-time communication in wireless sensor networks and real-time embedded systems.

Seong Hoon Kim received the B.S. and M.S. degrees in electronic and telecommunication engineering from Kangwon National University, Chuncheon, Korea, in 2006 and 2008, respectively. He is currently working toward the Ph.D. degree with the Computer Science Department, Korea Advanced Institute of Science and Technology, Daejeon, Korea.

His research interests include distributed real-time embedded systems, radio-frequency identification and sensor networks, and mobile/wireless communications.

Daeyoung Kim (M'98) received the B.S. and M.S. degrees in computer science from Pusan National University, Busan, Korea, in 1990 and 1992, respectively, and the Ph.D. degree in computer engineering from the University of Florida, Gainesville, in 2001.

He was a Research Staff Member with the Electronics and Telecommunications Research Institute, Daejeon, Korea, from January 1992 to August 1997. From September 2001 to January 2002, he was a Research Assistant Professor with the Arizona State University, Tempe. He was an Associate Professor with the Department of Computer Science and Engineering, Information and Communications University, Daejeon, from 2002 to 2009. Since March 2009, he has been an Associate Professor with the Department of Computer Science, Korea Advanced Institute of Science and Technology, Daejeon. He is a Director of Auto-ID Lab Korea (www.autoidlabs.org) and a Director of the Global Ubiquitous Sensor Networks National Research Laboratory. His research interests include sensor networks, real-time and embedded systems, and robotics.